Optimizing Data Volume Return for Ka-Band Deep Space Links Exploiting Short-Term Radiometeorological Model Forecast

Marianna Biscarini, *Member, IEEE*, Frank S. Marzano, *Senior Member, IEEE*, Mario Montopoli, Klaide De Sanctis, Luciano Iess, Maria Montagna, *Member, IEEE*, Mattia Mercolino, and Marco Lanucara

***Abstract*—The goal of this work is to demonstrate how the use of short-term radio-meteorological forecasts can aid the optimization of transferred data volumes from deep-space (DS) satellite payloads to Earth receiving stations. To this aim, a weather forecast (WF) numerical model is coupled with a microphysically oriented radiopropagation scheme in order to predict the atmospheric effects on Ka-band signals in DS links. A regional WFs model is exploited to obtain short-term predictions of the atmospheric state. The microphysically oriented radiopropagation scheme consists in a 3-D radiative transfer model which is used to compute the slant path attenuation and the antenna noise temperature at Ka-band in order to predict the signal-to-noise ratio at the receiving station. As a baseline, the BepiColombo mission to Mercury is chosen. Two prediction methods, statistical and maximization, are introduced and tested in two scenarios: 1) full-numerical scenario, where simulated data are used for evaluating the performances of the prediction techniques; 2) semiempirical scenario, where measured meteorological data are exploited to simulate beacon measurements in clear and rainy conditions. The results are shown in terms of received and lost data volumes and compared with benchmark scenarios. Using short-term radio-meteorological forecasts, yearly data volume return can be increased more than 20% if daily WFs, rather than monthly climatological statistics, are exploited.**

***Index Terms*—Deep space (DS) exploration, Ka-band downlink, numerical modeling, radiopropagation, WF.**

Manuscript received July 03, 2015; revised September 22, 2015; accepted October 20, 2015. Date of publication November 17, 2015; date of current version December 31, 2015. This work was supported in part by the Sapienza University of Rome and in part by the European Space Agency under the ESOC contract 4000107890 "Study of Ka-band downlink operation concept for BepiColombo based on the use of weather forecasts."

M. Biscarini, F. S. Marzano, and M. Montopoli are with the Department of Information Engineering, Electronics and Telecommunications (DIET) and CRAS, Sapienza University of Rome, 00184 Rome, Italy, and also with CETEMPS, University of L'Aquila, 67100 L'Aquila, Italy (e-mail: biscarini@diet.uniroma1.it; marzano@diet.uniroma1.it; montopoli@diet.uniroma1.it).

K. De Sanctis is with HIMET srl, 67100 L'Aquila, Italy (e-mail: klaide.desanctis@himet.it).

L. Iess is with the Department of Mechanical and Aerospace Engineering (DIMA) and CRAS, Sapienza University of Rome, 00184 Rome, Italy (e-mail: luciano.iess@uniroma1.it).

M. Montagna is with SciSys GmbH at ESOC, European Space Agency, 64293 Darmstadt, Germany (e-mail: maria.montagna@esa.int).

M. Mercolino and M. Lanucara are with ESOC, European Space Agency, 64293 Darmstadt, Germany (e-mail: mattia.mercolino@esa.int; marco.lanucara@esa.int).

Color versions of one or more of the figures in this paper are available online at http://ieeexplore.ieee.org.

Digital Object Identifier 10.1109/TAP.2015.2500910

I. Introduction

DEEP space (DS) exploration missions are aimed at acquiring information about the solar system and its origin and composition. To achieve this result, a significant communication capacity must be guaranteed to the spacecraft-to-Earth links [1], [2]. High communication link capacity is typically limited by the channel maximum bandwidth, the availability of the Earth-to-spacecraft visibility periods and the achievable signal-to-noise ratio. All these aspects introduce some limitations on the maximum bit rate usable for a given signal-to-noise ratio. In addition, the long distance involved in the Space-to-Earth links and the constraints imposed by orbital aspects and link geometry, feed the need for new optimization strategies of the Space-to-Earth links.

In this respect, the Ka-band (around 32–34 GHz) and higher frequency channels can provide an appealing capacity for DS missions especially if compared to the more commonly used X-band (around 8.4 GHz) [1]–[4]. Ka-band transmission can offer an advantage over X-band because of the squared-frequency law increase of antenna directivity of the downlink beam for the same antenna effective area (up to 12 dB). Moreover, at Ka-band, the bandwidth can be much higher than that at X band (up to 50 times). In this respect, the BepiColombo (BC) mission, the cornerstone mission to Mercury designed by the European Space Agency (ESA) and expected to launch in 2017 [3], is a DS satellite mission adopting a Ka-band transmission system operationally for the downlink at 32 GHz. The prime ground station of the BC mission will be in Cebreros (Spain) [5].

However, the Earth troposphere may impair the space-to-Earth carrier signals at frequencies higher than 10 GHz by degrading its integrity and thus reducing the channel temporal availability. The optimal allocation of channel resources above the X band is limited by the significant impact of radiometeorological factors, which can degrade the quality of service for fairly high percentage of time [4]. The major cause of outages at Ka-band and above is not only convective rainfall, as for lower frequencies, but even non precipitating clouds and moderate precipitation produced by stratiform rain events [6]. For Earth stations with low system temperature (which is usually the case for DS stations, such as the one in Cebreros), the impact of atmospheric noise temperature is not negligible [7], [9]. The specific attenuation due to cloudy and rainy troposphere can be much higher at Ka-band than at X band (e.g., order of 1.5–4.5 dB/km higher for rain rate ranging from 10 to

30 mm/h [4]. Thus, appropriate link margins should be allocated to take into account these atmospheric impairments and to reduce the target outage probability [1].

A strategy to face atmospheric impairments at Ka-band and above can be to adapt the channel availability to the predicted atmospheric state in order to maximize the transferred data volume [2], [6]. Weather forecast (WF) models can be used for this purpose, but only few studies have already treated the use of WFs for optimizing satellite communication at Ka-band [10]. One of the most comprehensive works in this respect has been that of Davarian *et al.* [2]. The results obtained in [2] have been considered promising, but probably not decisive to support the systematic exploitation of Ka-band data transfer links in DS missions [6]. Indeed, there are margins to improve the WF-based approach, especially by adopting a more accurate radiative transfer radiopropagation model in order to convert the forecasted meteorological variables into radiopropagation parameters [8], [9]. The advantage of this approach is that the latter are physically based and dynamically correlated to the evolving weather scenario rather than described by semiempirical relations. The drawback is mainly due to computational costs for the solution of the radiative transfer equations.

On the other hand, a numerical WF can be nowadays generated with finer spatial resolution than in the past, allowing a more detailed description of the state of the atmosphere affecting the radiopropagation channel. This goal can be reached by exploiting regional models where mesoscale atmospheric phenomena, including clouds and precipitation, are resolved with a resolution down to few kilometers (e.g., [11], [12]).

When considering an atmospheric state, which can influence the microwave propagation as at Ka-band, it is inevitable to consider its random variability at a spatial-temporal scale of kilometers and hours, respectively. This means that any attempt to describe the radiopropagation channel parameters should resort to a stochastic approach [2]. Moreover, the signal-to-noise ratio at the receiving station becomes a statistical variable of space-time random process representing the wave propagation through the troposphere [13]. The latter description is a generalization of the conventional approach where the slant path attenuation is characterized by the cumulative distribution function (CDF) and its value, exceeded for a given percentage of time, is used within the link budget formula [14].

A final issue to mention in the Ka-band exploitation for DS missions is related to the latency time required to activate the transmission plans. Space missions employ different operation plans spanning from long-term (months in advance) to medium-term (weeks) and there could be options for short-term planning cycles (few days or a day) when necessary [15]. The lower limit to the reduction of this latency time is set by the propagation signal delay between the ground station and the satellite. For very short-term predictions, also called nowcasting in meteorology applications, the temporal scales covered by the forecasts are of the order of few hours. The capability to perform a short-term operation plan can be coupled with the strategy to exploit a WF-based approach for short-term forecasts (i.e., weather prediction runs up to 24–48 h), taking into account that the accuracy of the latter tends to decrease with the increase of the lead time.

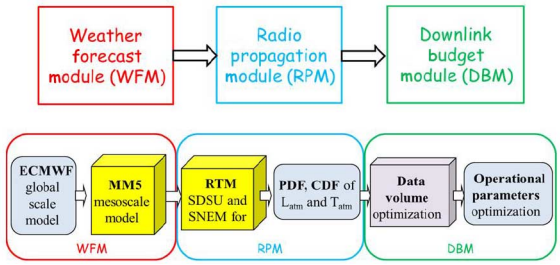

Fig. 1. Block diagram of the RadioMetOP chain. See text for details.

In order to address the open issues just discussed, the objectives of this work are: 1) to develop a simulation chain to predict Ka-band link budgets, based on physically based radio-meteorological models able to produce atmospheric statistics of signal path attenuation and sky noise temperature derived from short-term WF simulations on a daily basis; ii) to use the predictions of atmospheric statistics to maximize the received data volume during a satellite Earth-to-spacecraft visibility period by applying a stochastic approach; iii) to make a sensitivity analysis of the proposed physically based stochastic approaches and a preliminary verification of the WF-based methodology potentials in the DS radio-link analysis. The results obtained using the forecasted daily atmospheric statistics can be compared with those obtained using monthly long-term statistics derived by measurements collected for several years in the past (climatological statistics). All results are compared with a benchmark scenario that assumes perfect knowledge of the weather and the atmospheric state. The achievements, discussed in this document, are developed in the framework of the RadioMeteorological Operations Planner (RadioMetOP or RMOP) [15], [16], which is a program aimed at performing a feasibility study for the BC data link budget optimization, but can be easily extended to any space mission.

In order to satisfy the objectives of this work, we have organized the paper as follows. In Section II, we develop a model chain for the link budget simulation process composed by three modules: WF, radiative transfer, and downlink budget. In Section III, after describing the pass and subpass analysis, we explain the operational parameters optimization and data volume prediction techniques (statistical and maximization) based on a stochastic approach. In Section IV, a test procedure of the WF-based approach is shown for two case studies: 1) full-numerical scenario, to present a numerical sensitivity analysis; 2) semiempirical scenario, to evaluate a preliminary verification for the link design optimization. Finally, Section V is dedicated to a summary and to outline the possible future works to improve the proposed approach and to overpass its limitations.

II. RadioMetOP Architecture

The RadioMetOP processing chain is composed of three modules, as shown in Fig. 1.

1) WF module (WFM): devoted to the determination of the 3-D atmospheric parameters (temperature, pressure, humidity, liquid and ice water, hydrometeor microphysics) and their temporal evolution.

2) Radio propagation module (RPM): to properly convert WF outputs into the expected signals at the receiving Earth station in terms of path attenuation and atmospheric noise temperature at Ka band.
3) Downlink budget module (DBM): to optimize the operational parameters by way of stochastic techniques (Sections III-B and III-C). The latter are used for the evaluation of the atmospheric effects on DS Ka-band transmission and link design optimization. The term stochastic refers to the fact that the meteorological parameters, driving the link budget optimization, are assumed to be stochastic variables so that their statistics, in terms of CDF and probability density function (PDF), are involved in the link design optimization. The operational parameters are the transmission data rate (R_b) and the minimum elevation angle (θ_m) of the ground station pointing to the spacecraft antenna (Section III).

The outputs of the RadioMetOP chain are the optimal values of the operational parameters. The latter are generated at the same forecast time, i.e., with several hours in advance before the spacecraft-to-Earth data transfer is actually activated, thus enabling the possibility to generate a short-term planning to be used onboard the spacecraft.

The target area for this study is Cebreros (Spain), where the main BC receiving ground station is located. The period of interest is the year 2012 for which meteorological surface measurements at the Cebreros station are available and used as reference for estimating path attenuation and validate the WF approach. The use of WF models allows dealing with the most probable and continuously updated radio-meteorological 3-D scenario during the data transfer period, instead of relying on a monthly or yearly long-term statistics which can strongly penalize the available link margin due to its conservative choice. It is worth noting that, as already mentioned, the RadioMetOP chain describes a general methodology that can be used for any space mission by adapting the WFM inputs to those of the geographical area of interest.

A. Weather Forecast Module

Several numerical weather prediction models at mesoscale are available in literature, such as the Mesoscale Model 5 (MM5) [11], Weather Research and Forecasting (WRF) model [17], the Aire Limitée Adaptation Dynamique Développement International (Aladin) model [18], the Regional Atmospheric Modeling System (RAMS) [19], and the Consortium for Small-scale Modeling (COSMO) [20]. They are all nested within global-scale WF models that provide boundary conditions at the mesoscale domain of interest. For our purposes, we have decided to use the MM5 numerical model that can be considered the precursor of WRF. Both MM5 and WRF are among the most known and reliable WF models. The WRF model is thought to be more computationally efficient and it is recommended for predictions at high horizontal spatial resolution (i.e., 1–3 km). However, for a radiopropagation problem, we should consider that slant paths may cross the atmosphere for several kilometers or tens of kilometers (depending on the antenna elevation angle). A too high spatial resolution, on the one hand, might be useless since both attenuation and sky temperatures are path-integrated parameters and, on the other hand, might amplify the space–time WF prediction errors due to the difficulty to locate a convective system at the right time (so-called "double-penalty" WF error). In our study, the use of MM5 is justified because a horizontal spatial resolution of 6 km has been adopted as an acceptable compromise between spatial resolution and computational costs, being these quantities directly related.

The MM5 is a regional-scale and nonhydrostatic model developed by Pennsylvania State University and National Center for Atmospheric Research (PSU/NCAR) [11], [21]. The mesoscale forecast model is used to perform higher spatial resolution forecasts, including explicit microphysics, using a global-scale model as an input. The latter is used to provide initial (time) and boundary (space) conditions to the regional mesoscale model. RadioMetOP employs the European center for medium range weather forecast (ECMWF) data available every 12 h with a horizontal spatial resolution of 27 km and a temporal resolution of 6 h (Fig. 1). This model nesting allows to downscale the numerical weather prediction and to include explicit turbulence and convection schemes to provide a more realistic description of the boundary layer and cloud formation in terms of particle size distributions [19].

For cloud modeling, three microphysical parameterizations are available in MM5: Reisner 1 (R1) [11], Reisner 2 (R2) [22], and Goddard [12]. The R1 scheme accounts for cloud water (q_w), cloud ice (q_i), rain (q_r), and snow (q_s) mixing ratios to be produced simultaneously, but it does not account for the production of graupel. Instead, the Goddard and R2 schemes include one further prognostic equation for graupel (q_g). For all MM5 microphysical schemes, the size distribution of the hydrometeors is assumed to follow an inverse-exponential model

$$N_h dx = N_h^0 e^{-\lambda x} dx \tag{1}$$

where x is the particle size, h is a generic hydrometeor (i.e., $w,\ \text{water},\ i,\ \text{ice},\ r,\ \text{rain},\ s,\ \text{snow},\ g,\ \text{graupel}$), λ is the slope parameter, and N_h^0 is the intercept parameter. The parameter λ is inversely proportional to the mixing ratio of the any hydrometeor ($q_h \equiv q_w, q_i, q_r, q_s, \text{or } q_g$)

$$\lambda = \left(\frac{\pi \rho_h N_h^0}{\rho q_h}\right)^{1/4} \tag{2}$$

where ρ is the density of air and ρ_h is the density of any hydrometeor. From (2), the greater the mixing ratio is, the wider the size distribution. The intercept parameters N_h^0 are fixed for both the R1, R2, and Goddard schemes.

The MM5 output is the 4-D atmospheric state vector $\mathbf{x}_{\mathrm{atm}}$, defined for any grid point (x, y, z) and time t, including thermodynamic variables (e.g., pressure, temperature, humidity, wind velocity, and orientation) and microphysical variables (e.g., atmospheric particle concentration of liquid and water clouds and aerosol dispersions) on several pressure levels.

Within RadioMetOP context (BC mission), MM5 is set up to provide 1-to-5 days (24–120 h) forecast, starting at 00:00 UTC for the 2012 [15] and with a release period of 1 h. Note that

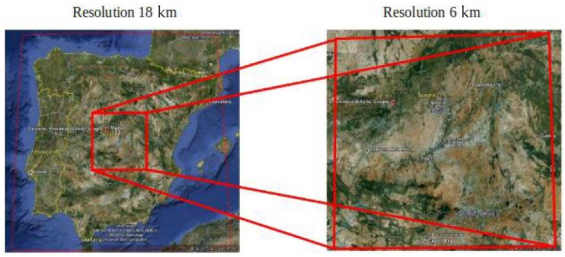

Fig. 2. Two nested domains adopted in the MM5 model.

the temporal resolution of the MM5 outputs is few seconds, but due to storage memory-problems, we have sampled the MM5 outputs every hour. We have used predictions with 24 h lead time (short-term daily forecast). The model has been performed considering two-way nested domains, as shown in Fig. 2. The two-way nesting implies that the first and second domain interact each other exchanging information. Starting from 27 km, the model resamples at 18 and 6 km for domain 1 and 2, respectively: the two regional domains are basically Spain and the area around Cebreros [15]. The vertical structure considers 22 vertical pressure levels unequally spaced, having higher resolution in the lower layers. The Medium Range Forecast [23], [24] parameterization for the Planetary Boundary Layer is used. The Kain-Fritcsh [25] cumulus convection parameterization is used for domain 1 and 2 (Fig. 2). R2 scheme supplies an explicit computation of microphysics. We have tested the MM5 predictions using meteo-gauge station data, available for the year 2012 in Cebreros. The model errors have been studied according to the three indexes probability of detection (POD), false alarm rate (FAR), and critical success index (CSI) with respect to a no-rain event [26]. Keeping in mind that the perfect detection corresponds to $\mathrm{POD} = \mathrm{FAR} = 100\%$ and $\mathrm{CSI} = 0\%$; we have found that the POD and the FAR are within 90% and 100%, whereas the CSI index is within 0% and 8% for one year of MM5 predictions (with 24-h lead time).

B. Radio Propagation Module

Among the radiative transfer solutions available in literature, we have adopted a radiopropagation model based on the Eddington radiative transfer approximation [8], [27]. Other possibilities, such as the Monte Carlo and finite-difference techniques [28], are too much onerous from a computational point of view and their advantages are expected to be negligible in this work [29].

The radiative transfer model (RTM) is the core of the RPM and computes the atmospheric path attenuation L_{atm} and the atmospheric equivalent noise temperature T_{atm}, taking into account the atmospheric state vector $\mathbf{x}_{\mathrm{atm}}$ generated by the MM5 model (as sketched in Fig. 3). Note that the RTM processes, each single vertical profile of the weather variables simulated by MM5. Thus, the spatial and temporal resolutions of the RTM outputs (L_{atm} and T_{atm}) are the same of those assumed in the MM5 forecasts and are expressed, as time series, for a given position (x, y) and several elevation angles (from 10° to 90° at step of 10°). For the link budget, we have computed the statistics of L_{atm} and T_{atm}, i.e., CDFs and PDFs, from their respective time-series.

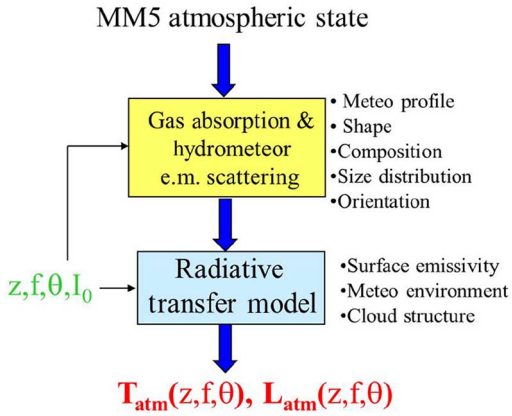

Fig. 3. Scheme of RTM data modeling and processing for a given receiving station (z = vertical height, f = frequency, θ = elevation angle, I0 = incident radiance, T_{atm} = atmospheric equiv. noise temperature or brightness temp., L_{atm} = path attenuation).

The RTM is largely used to simulate spectral radiances emitted and scattered by the atmosphere in different conditions (rainy, snowy, cloudy) [8], [29]. Radiances are usually expressed in terms of brightness temperatures through the Rayleigh–Jeans approximation of the Plank law [7]. The computational burden for computing the gas and hydrometeor electromagnetic scattering in the 3-D volume can be reduced by simplifying approximations, such as spherical shapes of particles, unpolarized radiance, and pseudo-3-D simulation geometry [27]. In this work, we have used a RTM, based on modules of the Satellite Data Simulator Unit (SDSU) [27] and Sky Noise Eddington Model (SNEM) [8], [9], [30]. SDSU-SNEM is a simulator that can produce synthetic radiances and path attenuation as measured by meteorological satellites and it has been adapted to ground-based microwave radiometers. Microphysical parameterizations of spherical particles have been properly set up in SDSU-SNEM using MM5 outputs for each grid point [27].

Differently from conventional approaches [31], SNEM-SDSU is able to characterize a thermally nonuniform and scattering atmosphere slab [9]. Since for ground-based measurements, the brightness temperature can be expressed through the effective or mean radiative temperature T_m, the formula can be inverted to express T_m (K) as follows [9]:

$$T_m(z=0,\theta) = \frac{T_B(z=0,\theta) - T_C e^{-\tau/\mu_0}}{1 - e^{-\tau/\mu_0}} \tag{3}$$

where z is the zenithal height above the surface and $z = 0$ is the surface level, T_B is the brightness temperature (K), T_c is the cosmic background temperature (about 2.73 K), τ is the vertical optical thickness (m^{-1}) (due to both absorption and scattering), $\mu_0 = \cos\ \theta$ where θ is the antenna elevation angle. We can derive the atmospheric slant-path attenuation A (dB) from T_m and radiometric measurement of T_B [9]

$$\begin{aligned} A(z=0,\theta) &= \frac{4.343}{\mu_0}\tau \\ &= 4.343 \cdot \ln\left(\frac{T_m(z=0,\theta) - T_C}{T_m(z=0,\theta) - T_B(z=0,\theta)}\right). \end{aligned} \tag{4}$$

A way to use the previous equation is to resort to the ITU-R model [31] where $T_m(z=0,\theta)=T_0=275$ K. Since this is a very rough approximation, in this work, we have used the Eddington formulation [8]. According to this model, the brightness temperature is expanded in terms of Legendre polynomials with respect to μ_0 and a closed-form expression for the ground-based effective mean temperature is obtained as a function of optical parameters under the hypothesis of an homogenous atmospheric slab and a temperature linear decrement [8], [9]

$$T_m(z=0,\theta)=f_{\mathrm{SNEM}}(\tau,\mu_0,w,g) \tag{5}$$

where f_{SNEM} is a single-value function, ω is the volumetric albedo, and g is the asymmetry factor [8]. The SNEM approximation and its use to develop a physically based parametric model for the sky-noise temperature are largely described in [32] and [30].

We have tested the radiative model using long-term statistics: CDFs of path attenuation published by the NASA Jet Propulsion Laboratory (JPL) [33].

C. Downlink Budget Module

The DBM is devoted to the computation of the downlink parameters (signal-to-noise ratio, frame error rate [FER], transmission data rate, received and lost frames).

In space radiocommunications, the classical link-budget method is based on imposing a link margin at the lowest elevation angle (typically 10° for DS missions) with the atmospheric conditions that guarantee a required weather availability given in terms of cumulative distribution (CD) [34]. This approach is successful at S and X band, but is not necessarily suitable at Ka-band due to the much larger atmospheric uncertainties at these frequencies [14]. A stochastic approach, based on the maximization of the data return in an average sense with the atmospheric loss being the driving random variable, has been introduced for Ka-band interplanetary links [2], [6], [13], [14]. Such approach requires reliable statistics for the atmospheric noise temperature and path attenuation to compute the link budget. The data return maximization approach (Section III-C) is the baseline link budget method considered in this work; the classical link budget approach (Section III-B) is also considered for comparison.

We can describe the power received at the end of a point-to-point link with a compact form of the Friis line-of-sight equation [13]

$$\frac{E_b}{N_0}(t)=f_{\mathrm{ENR}}\left\{C_{\mathrm{TRX}},\lambda,\theta(t),R_b,r,L_{\mathrm{atm}}(\mathbf{x}_{\mathrm{atm}}(t)),\right.$$
$$\left.T_{\mathrm{atm}}(\mathbf{x}_{\mathrm{atm}}(t))\right\} \tag{6}$$

where f_{ENR} is the free space equation for the energy-per-bit (E_b) to noise-density (N_0) ratio ($\mathrm{ENR}=E_b/N_0$), C_{TRX} is a cumulative quantity including all the transmitter/receiver parameters (such as the gain over system noise temperature rate, the modulation, and demodulation losses and the equivalent isotropic-radiated power), λ is the carrier wavelength, θ is the ground-station antenna elevation angle, R_b is the data transfer bit rate, r is the slant range between the Earth station and the spacecraft, $\mathbf{x}_{\mathrm{atm}}$ the atmospheric spatial state vector, L_{atm} is the atmospheric path loss, and T_{atm} the atmospheric equivalent noise temperature. Note that the elevation angle of the ground-station antenna is defined as the angle between the antenna boresight and the horizon (ranging from 0° at the horizon to 90° at the zenith). Note also that in (6) L_{atm} and T_{atm} do not depend on lambda, this because we are considering a narrow portion of the frequency spectrum (32 GHz), where we assume L_{atm} and T_{atm} independent from lambda. L_{atm} and T_{atm} are defined by CDFs and PFDs computed by the RPM.

During any visibility period between the satellite and the Earth station (that are the periods in which data transmission can take place), the FER, defined as the number of lost frames divided by the number of transmitted frames, should be calculated to have an indication of the quality of the transmission. FER is related to ENR in (6) through a known function f_{FER}, which depends on the channel coding adopted for the transmission

$$FER(t)=f_{FER}\left\{\frac{E_b}{N_0}[\theta(t),R_b(t),\mathbf{x}_{atm}(t)]\right\} \tag{7}$$

where we have reduced for simplicity the dependence of E_b/N_0 in (6) to the basic degrees of freedom.

Once FER(t) is known for each antenna pointing angle $\theta(t)$, we can calculate the number of the transmitted, lost and received frames, indicated by F_{TX}, F_{LX}, and F_{RX}, respectively. The computation of F_{TX}, F_{LX}, and F_{RX} is accomplished within each interval Δt of spacecraft-to-Earth line-of-sight.

We have carried out this computation by integrating the FER function on Δt [15], [16]

$$\begin{aligned}F_{\mathrm{TX}}(\Delta t)&=\frac{R_b}{r_B}\Delta t\\ F_{\mathrm{LX}}(\Delta t)&=\frac{R_b}{r_B}\int_{\Delta t}\mathrm{FER}(t)dt\\ F_{\mathrm{RX}}(\Delta t)&=F_{\mathrm{TX}}(\Delta t)-F_{\mathrm{LX}}(\Delta t)\end{aligned} \tag{8}$$

where r_B is the frame block length (in our case 8920 bit/frame) and Δt is the visibility time window (expressed in seconds). The total yearly data volume is obtained by summing together the received frames of the single visibility periods (Δt) of the year. We have distinguished two types of visibility periods: satellite passes and subpasses. They are defined as the periods when there is a line-of-sight between the ground station and the planet and between the ground station and the spacecraft orbiting around the planet, respectively. A more detailed explanation of passes and subpassed can be found in Appendix A.

Note that in (8), the transmitted frames are not integrated with respect to time because the bit rate R_b (in bit/s) is constrained to be constant in the period Δt; therefore, $F_{\mathrm{TX}}(\Delta t)$ is the function of constant parameters. The percentage fractional number of lost frames $F_{\mathrm{LX}\%}$ (equal to $100F_{\mathrm{LX}}/F_{\mathrm{TX}}$) can be an important parameter for optimizing closed-loop file transfer protocols [14]. The fact that $\mathbf{x}_{\mathrm{atm}}$ is a random vector variable in the space–time domain implies that FER fluctuates randomly in time and as a consequence F_{LX} and F_{RX} are random functions

as well. Thus, both F_{LX} and F_{RX} are characterized by PDFs indicated by $p_{\mathrm{LX}}(F_{\mathrm{LX}})$ and $p_{\mathrm{RX}}(F_{\mathrm{RX}})$, respectively. This consideration opens the possibility to derive the statistical moments of these stochastic processes such as their mean ($< >$) values: $< F_{\mathrm{LX}} >$, $< F_{\mathrm{RX}} >$.

The details of the data volume prediction methods implemented in the DBM are described in Section III.

For the aim of this study, we have implemented this module according to ESA link budget methods at Ka-band, but we adapted it to ingest radio-meteorological forecasts data given in the form of PDF for atmospheric attenuation and equivalent noise temperature. We have validated the module comparing the yearly data volumes derived from the ESOC link budget tool and using as atmospheric model the data published by the NASA/JPL already mentioned [14].

III. Data Volume Prediction and Optimization

The maximization of the received data volume in a DS mission has significant priority as a requirement. To achieve this aim, we can opt to maximize the expected received frames $< F_{\mathrm{RX}} >$ in average terms [13], [14]. The latter primarily depends on the transmission data rate R_b, chosen on the basis of the atmospheric attenuation in each visibility period Δt so that from (6) the lower the attenuation is, the higher the bit rate can be. Moreover, since the slant path attenuation decreases when the elevation angle increases, higher bit rates can be exploited for higher elevation angles (and vice versa). The bit rate is the first operational parameter to optimize in a link design: bearing in mind that R_b is constrained to be constant in Δt, higher R_b can be allowed for Δt characterized by higher elevation angles (see Section III-A and Appendix A). Therefore, the minimum elevation angle θ_m of the Δt period can also be optimized, together with the selection of an optimal constant value for R_b [14]. The optimization of such operational parameters, R_b and θ_m, is obtained pass per pass or subpass per subpass (Δt per Δt), thus leading to two analysis type: pass and subpass analysis (Section III-A). These analyses are accomplished by following two techniques: statistical and maximization technique (Sections III-B and III-C, respectively), based on exploiting the statistics of the atmospheric attenuation and equivalent noise temperature in terms of PDFs and CDFs. Both of them are constrained to dimension the link budget to have an ENR larger than a given threshold

$$\mathrm{ENR(t)} \geq \mathrm{ENR_{th}} \tag{9a}$$

$$\mathrm{ENR_{th}} = \mathrm{ENR_{tec}} + \mathrm{ENR_{tol}} \tag{9b}$$

where $\mathrm{ENR_{th}}$ is the threshold for the E_b/N_0 given by the sum of the technology ($\mathrm{ENR_{tec}}$) and system tolerance ($\mathrm{ENR_{tol}}$) thresholds. $\mathrm{ENR_{tec}}$ and $\mathrm{ENR_{tol}}$ depend on the adopted coding scheme for the transmission and the required tolerance, respectively. In this work, we have set $\mathrm{ENR_{th}}$ to 3.3 dB by including technology/coding threshold for Turbo Code $\frac{1}{14}$($\mathrm{ENR_{tec}} = 0.3$ dB, that corresponds to an FER below 10^{-5}) and system tolerance ($\mathrm{ENR_{tol}} = 3$ dB).

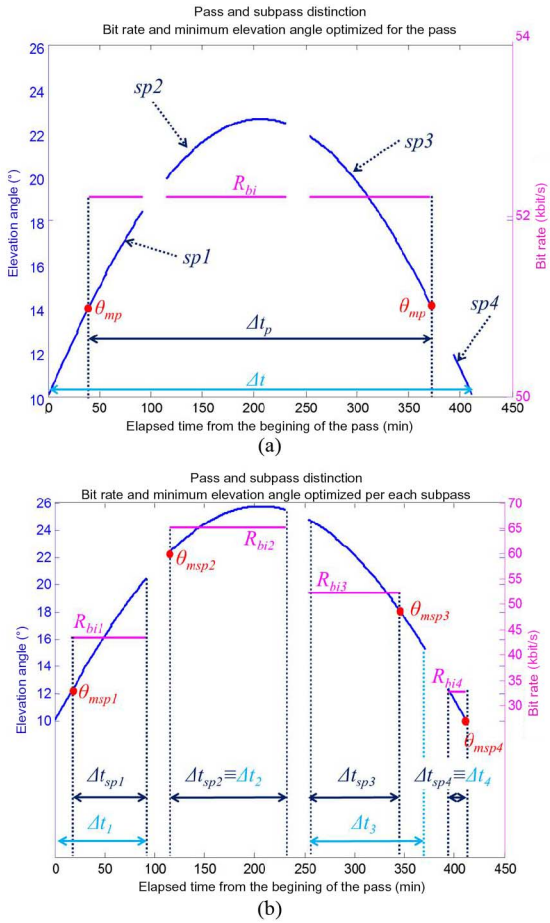

Fig. 4. (a) Pass analysis. (b) Subpass analysis. See text for details.

A. Pass and Subpass Data Processing

Fig. 4 shows an example of pass (in panel a) and subpass analysis (in panel b). In each panel, a single pass, composed by four subpasses ($spj, j = 1, 2, 3, 4$) is shown. During the nonvisibility periods (empty spaces) no transmission takes place and the bit rate is always set to zero. Each effective transmission period Δt_y (with $y = p$ or $y = sp$ for pass or subpass analysis, respectively), is characterized by the optimal couple (R_b, θ_{my}) representing the bit rate selected in the analyzed period Δt and the minimum angle where starting or ending the transmission in Δt. Note that the effective period Δt_y can be different from the analyzed period Δt since the latter real period of the analyzed pass or subpass, whereas the former is defined after the link budget analysis is carried out and θ_{my} is chosen. Since the number of data rates available to the BC mission is limited, R_b can assume only values taken from a given discrete set of data rates. Hereafter, we will refer to R_{bi} as the the ith discrete value of R_b within the BC data rate set.

In a pass analysis, R_{bi} is constrained to be constant for the whole pass, as shown in Fig. 4(a). The minimum elevation angle, which has to be optimized, coincides with the angle (θ_{mp}) where to start and stop the transmission during the pass. The time-slot of the pass effectively dedicated to the data transmission Δt_p is then defined by the angle θ_{mp} [as in Fig. 4(a)]. A higher θ_{mp} allows using a higher bit rate with respect to the

bit rate that would be used if the transmission were began at the horizon minimum elevation angle of the pass (i.e., 10°).

In a subpass analysis, R_{bi} is constrained to be constant in each subpass allowing step variations from two contiguous subpasses [see Fig. 4(b)]. The optimization of the minimum elevation angle θ_{msp} is carried out for each subpass. In the subpass analysis, we must distinguish between ascending and descending subpasses: a subpass is ascending when the elevation profile during the subpass increases with time (i.e., when it is positioned in the first half of the pass profile), it is descending when the elevation profile during the subpass decreases with time (i.e., when it is positioned in the second half of the pass profile). For subpasses positioned between the first and the second half of the pass (such as *sp2* in Fig. 4), our convention is to classify the subpass as ascending if the physical elevation angle at which the subpass starts (i.e., the angle where the visibility of the subpass starts) is lower than the physical angle at which the subpass ends (i.e., the angle where the visibility of the subpass ends) and vice versa. Thus, in Fig. 4, *sp1* and *sp2* are ascending subpasses, *sp3* and *sp4* are descending subpasses.

In a subpass analysis, θ_{msp} has two different meaning depending on ascending or descending subpasses. For the ascending subpasses, θ_{msp} is the angle where the transmission starts, whereas for descending subpasses θ_{msp} is the angle where the transmission ends. The time slot effectively dedicated to the data transmission Δt_{sp} is then defined by the angle θ_{msp} and the physical angle of end or beginning of the subpass in case of ascending or descending subpass, respectively [Fig. 4(b)]. As for the pass analysis, the optimization of the angle θ_{msp} allows using a higher bit rate with respect to the bit rate that would be used if the transmission were began (for ascending subpasses) or ended (for descending subpasses) at the physical minimum elevation angle of the subpass.

Note that the optimization of the minimum elevation angle can be more useful for subpasses characterized by lower elevation angles (i.e., where the slant path attenuation is more penalizing). For example: in Fig. 4(b), the optimization is useful for the *sp1*, but it is not for the *sp2* because the selected R_{b2} is already the maximum usable in *sp2* with θ_{msp2} that coincides with the physical beginning of the subpass (that means $\Delta t_2 = \Delta t_{sp2}$). Therefore, in the subpass *sp2*, it is useless to increase further the minimum elevation angle (and reducing the transmission period Δt_{sp2}). The definition of the visibility period Δt, within which we can optimize the operational parameters, comes out directly from Fig. 4. In a pass analysis Δt is defined as the temporal interval of the analyzed pass period: in Fig. 4(a), this period goes from minutes 0–407. In a subpass analysis, Δt is defined as the temporal interval of the considered subpass period. In Fig. 4(b): Δt for *sp1* is in the minutes 0–90, for *sp2* in the minutes 110–230, for *sp3* in the minutes 255–360, and for *sp4* in the minutes 395–407.

The computation of the received and lost frames is done considering the couple (R_{bi}, θ_{my}) for each effective transmission period Δt_y. Thus, the optimization problem reduces to find the optimum couple (R_{bi}, θ_{my}) in each period, Δt_y is a function of the random variable $\mathbf{x}_{\rm atm}(t)$ [16]. The outcome of the optimization procedure are the discrete temporal profiles $R_{bi}(t), \theta_{myi}(t)$ for all the· Δt_y of a selected period (i.e., 1 year in our case).

B. Statistical Technique ($\mathrm{CDF} = 90\%$*)*

The statistical technique implements the classical link budget approach, based on the ENR margins at the lowest elevation angle, with atmospheric conditions that guarantee a certain link availability, in this case 90%. The steps of the statistical algorithm schematically are as follows.

Step 1) Fix the probability of weather availability $p_{\rm atm}$ of the CDF for the variables $L_{\rm atm}$ and $T_{\rm atm}$ (respectively, $p_{\rm atm} = c_L(l_{\rm atm})$ and $p_{\rm atm} = c_T(t_{\rm atm})$) so that the values $l_{\rm atmp}$ and $t_{\rm atmp}$ are derived as inverse CDF: $c_L^{-1}(p_{\rm atm}) = l_{\rm atmp}$ and $c_T^{-1}(p_{\rm atm}) = t_{\rm atmp}$. Note that $l_{\rm atmp}$ and $t_{\rm atmp}$ must be computed at the antenna elevation angle θ_{my} (see point 4) and $p_{\rm atm}$ is here set to 0.9.

Step 2) The adopted CDF depends on the considered scenario (Sections IV-B and IV-C) and is derived from the WF analysis or from long-term statistics;

Step 3) Set the $\mathrm{ENR}_{\rm th}$ as in (9b), in our case being $\mathrm{ENR}_{\rm tec} = 0.3$ dB and $\mathrm{ENR}_{\rm tol} = 3$ dB.

Step 4) Vary the values of R_{bi} and θ_{my} consistently with (6) so that the following equation is satisfied:

$$\frac{E_b}{N_0} = \left.\frac{E_b}{N_0}\right|_{\theta=\theta_{my}, R_b=R_{bi}, L_{\rm atm}=l_{\rm atmp}, T_{\rm atm}=t_{\rm atmp}} \tag{10}$$

for all the possible combinations of (R_{bi}, θ_{my}) obtained by varying θ_{my} within the temporal profile $\theta(t)$ of Δt and R_{bi} within the BC discrete set.

Step 5) Among the values identified in the previous step, find the couples (R_{bi}, θ_{my}) which satisfy the constraint in 9(a).

Step 6) For all couples (R_{bi}, θ_{my}) obtained in step 4), compute $F_{\rm TX}(\Delta t_y)$ using (8) where Δt must be replaced with the Δt_y corresponding to the optimized θ_{my}. The final optimal solution is then found selecting the couple (R_{bis}, θ_{mys}) that maximizes the transmitted frames $F_{\rm TX}$ (the subscript "s" stands for "statistical" solution).

The selection of the solution couple is performed only considering the transmitted frames and a guaranteed weather link availability. The evaluation of the *expected* received and lost frames is carried out *a posteriori* (after the computation of the optimal couple R_{bis}, θ_{mys}) in a statistical manner by calculating the statistical average of the FER employing its PDF $p_{\rm FER}$

$$< \mathrm{FER}(\Delta t_y) > = < \int_{\Delta t_y} \mathrm{FER}(t)dt > \tag{11a}$$

$$< \int_{\Delta t_y} \mathrm{FER}(t)dt > = < f_{\rm FER}\{\mathrm{ENR}(\theta(\Delta t_y), R_{\rm bis}, L_{\rm atm}(x_{\rm atm}(t)), T_{\rm atm}(x_{\rm atm}(t))\} > = \int_0^\infty f_{\rm FER} p_{\rm FER}(f_{\rm FER}) df_{\rm FER} = \int_0^\infty f_{\rm FER}(l_{\rm atm}) p_L(l_{\rm atm}) dl_{\rm atm}. \tag{11}$$

(11b)

Note that, due to the dependence of the FER on both $L_{\rm atm}$ and $T_{\rm atm}$, a joint distribution of $L_{\rm atm}$ and $T_{\rm atm}$ should be introduced. However, for simplification of the overall methodology, we have considered $T_{\rm atm}$ as a dependent variable of $L_{\rm atm}$ [32]. The fourth equality in (11b) is possible thanks to a probability matching between $p_{\rm FER}$ and the PDF of the path attenuation $p_L(l_{\rm atm})$ as it holds

$$\mathrm{p_{FER}(f_{FER})df_{FER}} = \mathrm{p}_L(\mathrm{l_{atm}})\mathrm{dl_{atm}}. \tag{12}$$

The expected average received, lost and percentage of lost frames $< F_{\rm RX} >, < F_{\rm LX} >, < F_{\rm LX\%} >$ are calculated by means of

$$\begin{aligned} &< F_{\rm LX}(\Delta \mathrm{t_y}) > = < \mathrm{FER}(\Delta t_y) > \cdot (R_b/r_B) \\ &< F_{\rm LX\%}(\Delta t_y) > = < F_{\rm LX}(\Delta t_y) > \frac{100}{F_{\rm TX}(\Delta t_y)} \\ &< F_{\rm RX}(\Delta t_y) > = F_{\rm TX}(\Delta t_y) - < F_{\rm LX}(\Delta t_y) > \end{aligned} \tag{13}$$

where the term $F_{\rm TX}(\Delta t_y)$ is derived by the first of (8) with $\Delta t = \Delta t_y$. As already mentioned, the transmitted frames $F_{\rm TX}(\Delta t_y)$ are not averaged because, once the periods Δt_y are known, they are fixed and are not function of the random variable $\mathbf{x}_{\rm atm}(t)$.

C. Maximization Technique ($\mathbf{FLXth} = 5\%$)

The maximization technique optimizes the average number of received frames, while guaranteeing that the percentage of average lost frames does not exceed a given threshold, in this case 5%. The average values are computed as function of the atmospheric statistics. The steps of the maximization technique schematically are as follows.

Step 1) Consider the PDFs of path attenuation/sky-noise temperature (respectively, $p_L(l_{\rm atm})$ and $p_T(t_{\rm atm})$, which depend on the considered scenario (Sections IV-B and IV-C) and is derived from the WF analysis or from long-term statistics. Note that here we have to consider the whole PDF, for both $L_{\rm atm}$ and $T_{\rm atm}$, whereas in the statistical method just the knowledge of the CDF value at the probability of $p_{\rm atm}$ was needed.

Step 2) Set the desired E_b/N_0 (ENR) to the given threshold $\mathrm{ENR_{th}}$ as in point 2 of the statistical method.

Step 3) Set a maximum threshold for the percentage of lost frames FLXth for the time interval Δt_y. This threshold is related to the retransmission process, in our case $\mathrm{FLXth} = 5\%$.

Step 4) Consider all the possible combinations of (R_{bi}, θ_{my}) obtained by varying θ_{my} within the temporal profile $\theta(t)$ of Δt and by varying R_{bi} within the BC discrete set. For each of these couples, compute $<$ FER$(\Delta t_y) >$ and the expected $<$ FRX$(\Delta t_y) >$, $<$ FLX$(\Delta t_y) >$, $<$ FLX%$(\Delta t_y) >$ using (11)–(13).

Step 5) From the (R_{bi}, θ_{my}) couples obtained at step 4), select the optimal couple (R_{bim}, θ_{mym}), where the subscript "m" stands for "maximization" solution, that optimizes the expected number of average received frames and, at the same time, under the constraint in (9), produces a percentage of lost frames lower than the threshold FLXth fixed at step 3)

$$\begin{cases} [R_{bim}, \theta_{mym}] = \max_{\theta_{my}, R_{bi}} \{< F_{\rm RX}(\Delta t_y) >\} \\ < F_{\rm LX\%}(\Delta t_y) > \quad \leq \quad F_{\rm LXth}. \end{cases} \tag{14}$$

Note that selecting the optimum couple (R_{bim}, θ_{mym}) implies selecting the corresponding expected lost and received frames already computed in the previous step 4) (differently from the statistical technique that implies an *a posteriori* computation of the expected frames).

In the statistical method, the constraint in (9) is imposed just for one value of E_b/N_0: for $c_L(l_{\rm atm}) = p_{\rm atm}$ and for the minimum elevation angle (that is the worst case for the slant path attenuation). On the contrary, in the maximization approach, the whole PDF of $L_{\rm atm}$ is taken into account.

Note that in this maximization technique, the computation of the expected received and lost frames is carried out together with the optimization procedure of the operational parameters (whereas in the statistical case it is done *a posteriori*).

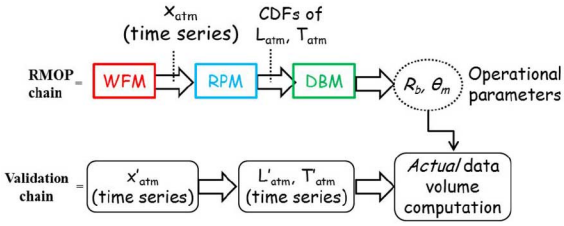

Fig. 5. Scheme of the validation chain. xatm, $L_{\rm atm}$, $T_{\rm atm}$ are the predicted weather conditions, x'atm, L'atm, T'atm are the actual weather conditions.

IV. Validation of the WF-Approach and Results

In this section, we will show the numerical results obtained from the RMOP proposed link budget estimation techniques using different scenarios. The final goal of our analysis is to exploit the predictability of radio-meteorological scenarios to maximize the received data volume within Ka-band downlink operations.

In order to evaluate the performances of the optimization methods and to validate the WF-approach, we have defined two reference weather scenarios. From each reference scenario, we have computed the actual received and lost frames, which are different from the expected ones. The actual frames are calculated from (8) when considering the selected $R_{bi}(t), \theta_{myi}(t)$ operating in the actual weather scenario for the period of interest (Sections IV-B and IV-C). The actual weather scenario is intended in terms of time series of attenuation and sky noise temperature (as explained in Fig. 5).

Two reference scenarios have been identified, depending on the dataset adopted to produce the time series of the actual weather conditions: full-numerical and semiempirical scenario. The former uses the time series coming from WF, whereas the latter uses time series of measured weather data, coming from the meteo-gauge station in Cebreros, then converted into synthetic path attenuations employing a simplified radiative model (SRM).

TABLE I
EXTRAPOLATION OF QUANTITIES IN FIG. 5

RMOP chain		Validation chain		
Quantity	Data source	Quantity	Data source: Full numerical	Data source: Semi empirical
x_{atm} (ts[1])	MM5	x'_{atm} (ts[1])	MM5	Meteo-gauge station
$L_{\text{atm}}, T_{\text{atm}}$ (ts[1])	RTM	$L'_{\text{atm}}, T'_{\text{atm}}$ (ts[1])	RTM	SRM
$L_{\text{atm}}, T_{\text{atm}}$ (PDF, CDF)	RTM[2] JPL tables[3]	–	–	–

[1]ts, time series.
[2]Time series then converted into PDFs and CDFs.
[3]Long-term climatological statistics published by the NASA-JPL [33]: monthly CDFs obtained collecting radiometric measurements at the NASA DS site of Robledo (40 km far form Cebreros) for 19 years in the past (September 1990–January 2009).

The analysis results are compared with an unconstrained case (benchmark) where some parameters are free to vary. The benchmark test case is defined as the ideal transmitting approach with no system constraints: fully adaptive R_b (changeable at each antenna elevation angle step), fulfilling the required minimum ENR ($\mathrm{ENR_{th}}$) in presence of a perfect forecast (error-free prediction of rainfall and attenuation time series). Results will be shown by applying both statistical and maximization techniques for both full-numerical and semiempirical scenario and the advantages of using WF models with respect to long-term statistics will be assessed.

In this work, the BC mission to Mercury has been taken as reference test case: the year 2021 is taken as reference for the antenna temporal elevation profile information since the satellite arrival to Mercury has been assumed to be at the end of 2020. Consequently, we have derived the satellite orbital data (with pass and subpass information) relative to the year 2021 using BC ephemeris. In order to perform this study and due to the need of a meteorological scenario for the year, we have associated the temporal elevation profile $\theta(t)$ for 2021 with the atmospheric state $\mathbf{x}_{\mathrm{atm}}(t)$ simulated by WF prediction model for the year 2012, for which surface meteorological measurements in Cebreros were available. In this way, we have constructed an antenna observation scenario and the corresponding atmospheric state. Considering the variability of the latter, this assumption should not reduce the validity of our numerical results in terms of received data volumes.

In Table I, we summarize the possible ways of extrapolating the quantities of Fig. 5 as functions of the considered scenario. The combination $(\mathrm{MM5} + \mathrm{RTM})$ in the RMOP chain correspond to the WF-approach. Note that in this work, meteo-gauge data in Cebreros were available with a sampling period of 1 min for the year 2012. Thus, we have set MM5 to give daily WF simulations for Cebreros with a sampling period of 1 h in the year 2012.

Even though the presented results are referred to our case study, i.e., the BC mission, the proposed methodology is quite general. Moreover, the computed data volumes do not refer to an operational contest but to simulated cases only.

A. Available Data and Constraints

For the link budget computation, we need to specify the input data for the target location and the period of interest. The input data to RMOP chain are:

1) the antenna elevation profile $\theta(t)$ (°), the slant distance r (km), and the blockages information (defining passes and subpasses periods) for the test period;
2) time series of the surface data in the area of Cebreros (to derive $\mathrm{x_{atm}}$): rain rate (mm/h), temperature (K), pressure (Pa), relative humidity (%);
3) time series of L_{atm} and T_{atm};
4) statistics of L_{atm} and T_{atm} (in terms of CDF or PDF) for data volume prediction.

Once the input parameters are defined, some mission-related constraints must be fixed before starting the analysis.

1) The bit rate R_{bi} must be selected within the BC discrete set of values.
2) R_{bi} must be constant within each pass or subpass Δt_y.
3) $\mathrm{ENR} \geq \mathrm{ENR_{th}}$ as in (9) where $\mathrm{ENR_{th}} = 3.3$ dB in our case.
4) $\mathrm{FLX}\%(\Delta t_y) \leq \mathrm{FLX_{th}}\%$ as in (14) with $\mathrm{FLX_{th}}\%$ set to 5% in our case. Note that in the statistical technique, this constraint is not imposed during the optimization process (as in the maximization technique), but it is verified *a posteriori*.
5) The optimization of the operational parameters must be carried out at least 1 day before the beginning of the upcoming pass or subpass.

For what concerns the atmospheric statistics, we will use PDF or CDF of atmospheric attenuation focusing on monthly and daily statistics. During the link budget optimization, for each analyzed period Δt, we will consider the PDF/CDF of the month or the day to which Δt belongs. The climatological statistics published by JPL are directly available as monthly CDF tables (and daily statistics are not available).

For what concerns the WF statistics, they are computed from the forecasted time series on daily basis. The WF-derived daily statistics are updated daily considering the forecasts for the day ahead with respect to the prediction time. The WF-derived monthly statistics are obtained by grouping the daily WF time series for each calendar month, as usually done for building statistics from measured data, and then converted into CDF and PDF.

B. Full-Numerical Scenario: Tests for Sensitivity Analysis

In this scenario, PDF statistics are computed from WF data for the link budget analysis. The WF time series (from which the PDF have been computed) are used to simulate the actual weather conditions for the actual data volume computation. This scenario is a useful laboratory to compare the different prediction approaches with the benchmark case.

Figs. 6 and 7 show the results for the subpass analysis for the statistical and the maximization approach, respectively, by comparing monthly and daily forecast statistics. In the left panels, received frames are plotted: note that the benchmark, by definition, is always the upper bound and that the curve relative

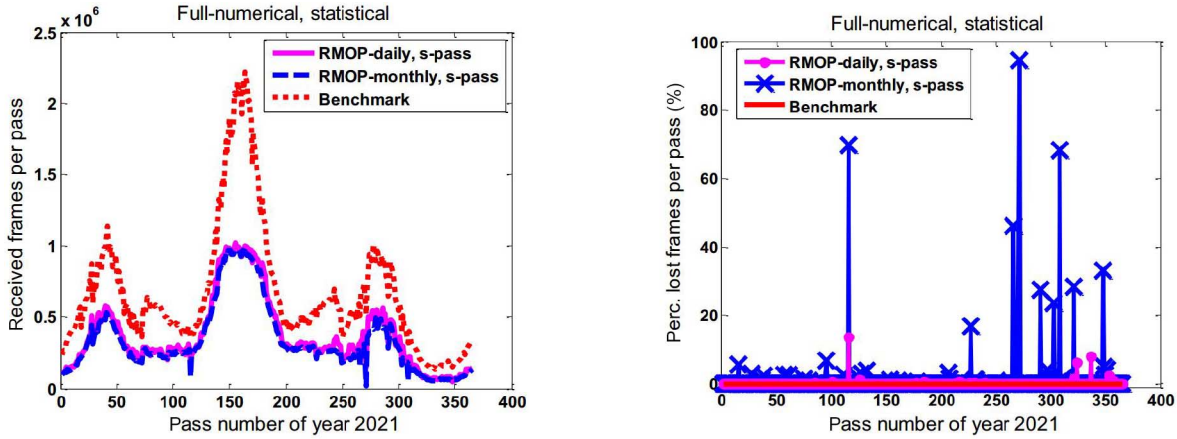

Fig. 6. Full-numerical scenario, statistical technique for subpass analysis. Left panel: received frames per pass obtained with monthly and daily statistics. Right panel: lost frames per pass obtained with monthly and daily statistics. Benchmark curve is also shown.

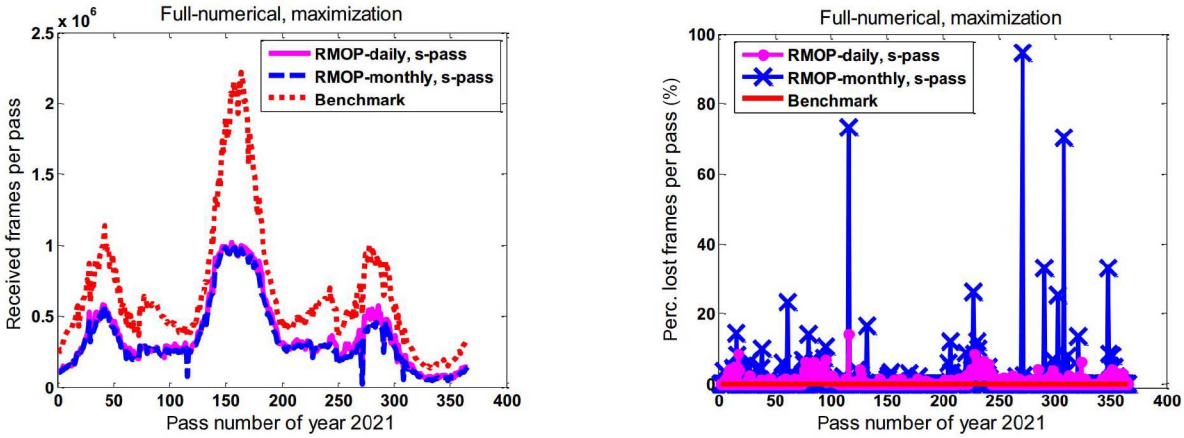

Fig. 7. Same as in Fig. 6, but for the maximization technique.

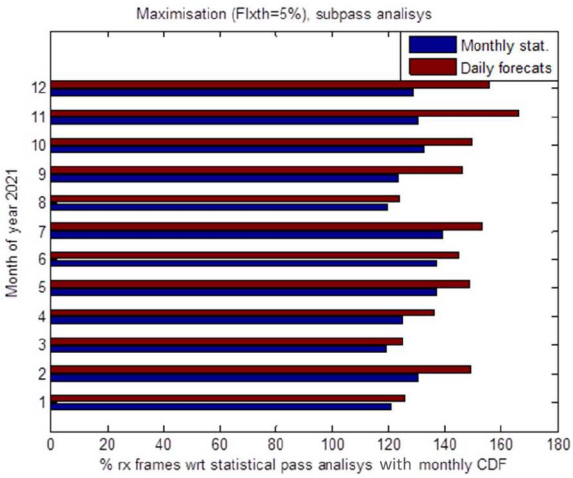

Fig. 8. Full-numerical scenario, maximization technique for subpass analysis. Monthly data volume: daily statistics are more convenient in rainy months.

TABLE II
FULL-NUMERICAL SCENARIO: YEARLY RECEIVED (RX) DATA VOLUME (DV) WITH STATISTICAL AND MAXIMIZATION TECHNIQUE FOR PASS AND SUBPASS ANALYSIS TYPE

Technique	Database, timescale, analysis type	Yearly rx DV (%)[(a)]	Yearly mean losses (%)
Statistical (CD=90%)	RMOP *Monthly*: pass	ref	0.73
	RMOP *Daily*: pass	110.2	0.06
	RMOP *Monthly*: s-pass	122.1	0.96
	RMOP *Daily*: s-pass	133.2	0.05
Maximization (F_{LXth}=5%)	RMOP *Monthly*: pass	107.0	3.73
	RMOP *Daily*: pass	111.2	3.72
	RMOP *Monthly*: s-pass	124.7	1.66
	RMOP *Daily*: s-pass	134.1	0.70
Benchmark	*Actual time series*: fully adaptive	179.2	0%

[(a)] Received data volume: percentage wrt reference case (ref).
Results with RMOP monthly and daily data are compared. Benchmark case is also shown.

to the daily statistics is generally higher than the one relative to the monthly statistics. In the right panels, lost frames are plotted: the benchmark always gives zero losses. The peaks in the lost frames with RMOP-monthly data corresponds to peaks of the actual attenuation time series (usually highest peaks are due to peaks of rain). Note that using RMOP-daily statistics the losses are much more controlled.

In Fig. 8, the received data volume for the different months is shown (the percentage is respect to the reference case: statistical technique, pass analysis with monthly CDF). The convenience

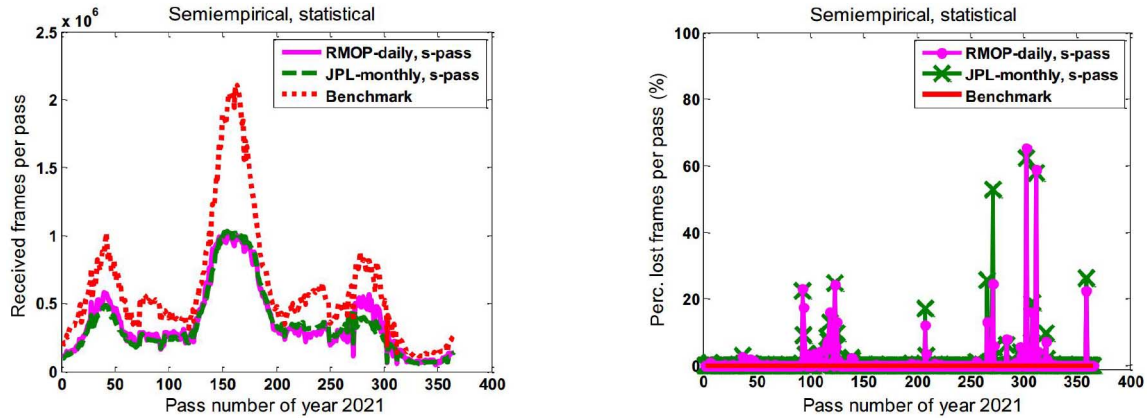

Fig. 9. Semiempirical scenario, statistical technique for subpass analysis. Left panel: received frames per pass obtained with monthly and daily statistics. Right panel: lost frames per pass obtained with monthly and daily statistics. Benchmark curve is also shown.

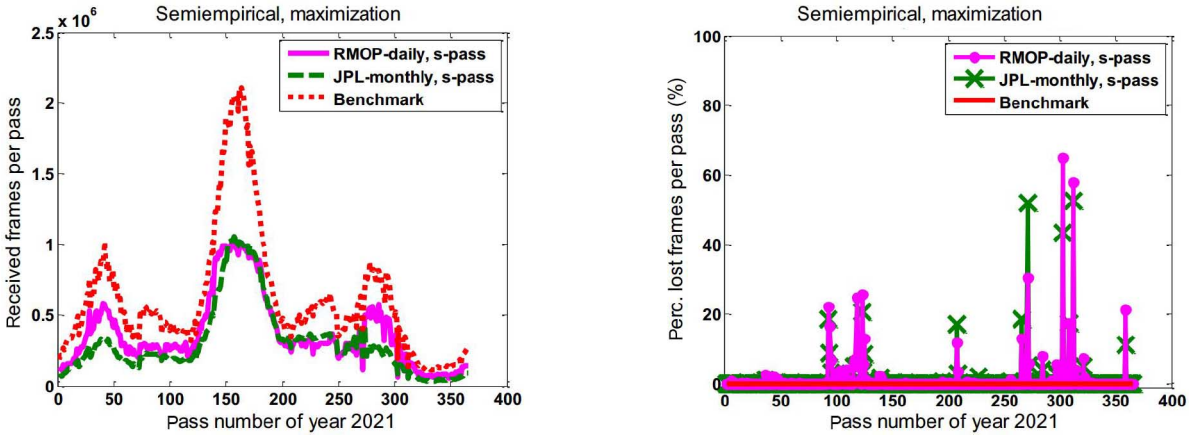

Fig. 10. Semiempirical scenario, statistical technique for subpass analysis. Left panel: received frames per pass obtained with monthly and daily statistics. Right panel: lost frames per pass obtained with monthly and daily statistics. Benchmark curve is also shown. Same as in Fig. 9, but for the maximization technique.

of using daily statistics is evident especially during the rainy months. The figure shows the maximization case but similar results are found for the statistical case too.

Table II reports the numerical results both for pass and subpass analysis, for both the statistical and maximization technique, compared with the benchmark case. Received data volume is expressed in percentage with respect to the reference case which is assumed to be the statistical technique using monthly RMOP data and pass analysis.

From previous figures and tables we can notice that:

1) predictions based on daily PDFs seem to be advantageous with respect to those based on monthly PDFs;
2) the increase in yearly data volume is mainly due to a reduction of lost frames rather than to a different data rate profile. This consideration stems from Figs. 6 and 7 where the curves of monthly-PDF and daily-PDF received frames are very similar as opposite to those of the lost frames;
3) lost frames can be better controlled using daily-PDF based predictions than monthly-PDF-based ones (second panel in Figs. 6 and 7);
4) the gain of daily-PDF-based predictions is larger in rainy months (see Fig. 8).

C. Semiempirical Scenario: Simulated Operational Case

In this scenario, the time series of the actual weather conditions are obtained from measured data. This is a sort of simulated operational scenario, useful to make a preliminary verification of the link budget computation and WF-based approach. The latter must be compared to the classical operational planning that could be used for BC, i.e., setting of the link parameters by considering long-term atmospheric statistics.

Unfortunately, we have not at disposal neither Ka-band beacon measurements at Cebreros nor ground-based radiometric observations. We have computed $L_{\rm atm}$ and $T_{\rm atm}$ using an SRM approximating $\mathbf{x}_{\rm atm}$ with surface measured data (pressure, temperature, humidity, and rain rate) derived from minute-scale meteo-gauge measurements in Cebreros.

The assumptions of SRM, useful to exploit surface measurements, can be summarized by:

1) horizontally stratified atmosphere;
2) standard atmosphere with standard profiles of pressure, temperature and humidity, parameterized to surface meteorological measurements;
3) single rain slab up to zero thermal height, estimated from surface temperature, and standard vertical thermal gradient;

4) specific attenuation power–law model depending on rain rate R (from ITU-R and SNEM simulations);
5) gas absorption derived from meteorological profiles
6) no cloud liquid water supposed in the atmosphere since no correlation with surface data can be used.

For the rain attenuation, the SRM method is based on SNEM simulations [32], tuned to meteorological conditions of Cebreros (instead of data obtained from standard ITU procedures and database [34]). To complete the gaseous part of SRM and compute the total attenuation (gas + rain), we have used the models illustrated in [7] replacing the standard surface data with the ones measured in Cebreros. In the SRM model, the effects of melting layer [35], ice particles, and hails are neglected. These aspects can lead to an underestimation of path attenuation values obtained from the SRM model, but any further model assumption could introduce a bias due to unknown conditions.

We have applied the statistical and maximization prediction techniques with two different data sets.

1) RMOP WF data: monthly and daily timescale statistics derived from forecasts in Cebreros for the year 2012.
2) JPL monthly statistics: CDF of path attenuation in Robledo [33].

Figs. 9 and 10 show results for subpass analysis, respectively, for both the statistical and maximization technique, comparing JPL-monthly statistics and RMOP-daily forecast. The same considerations of Figs. 6 and 7 can be applied but in this case, the convenience of using daily WF statistics is more evident, especially in the received frames with the maximization technique (Fig. 10, left panel) where the RMOP daily curve of the received frames is mostly higher than the JPL-monthly one. The reason is that, in the semiempirical scenario, the use of daily WF statistics allows to dimension the link budget with more precision: received frames computed with WF-daily statistics are higher compared to the received frames computed with climatological monthly statistics because the transmitted frames are higher (whereas, as shown in the right panel of Fig. 10, the lost frames are similar for the two cases). This means that dimension a link budget using WF-daily statistics permits a better selection of the optimum temporal profile of the couple (R_{bi}, θ_{myi}). This confirms that daily statistics obtained for the specific analyzed day are more reliable than monthly climatological statistics.

In Table III, we have reported numerical results in the same form of Table II, but for semiempirical scenario. The convenience of using daily forecast with respect to monthly statistics is again evident in terms of received data volume.

When JPL data are used, the statistical technique seems to be better than the maximization one differently from what happens with the RMOP data. But, the statistical technique does not provide a control of the losses since there is not an imposed threshold F_{LXth}. The practical effect of this lack of control is that, in an operational contest, the statistical technique is unacceptable because could lead to severe losses data in a single subpass, as shown in Fig. 11.

The fact that with RMOP data the maximization technique results to be better than the statistical one is due to the different behavior of the PDF curves, as shown Fig. 12. The JPL-CDF curves of attenuation have a much larger dynamics and this strongly influences the link budget computation with the maximization technique. Note that the JPL tables provide CDF values for attenuation until 99.0%, the missing values (up to 99.9%), necessary to compute PDF from CDF, have been extrapolated. Differently, RMOP CDF and PDF curves are directly computed from RMOP time-series. The different dynamics, in addition to the different spatial and temporal resolutions, is probably due to the fact that JPL statistics are obtained collecting data for 19 years, whereas RMOP statistics are obtained from simulations of one single year.

In Table IV, final important results are pointed out. The table compares the three principal estimation methodologies, highlighted in Table III. In the first line, there is the standard methodology for data return estimation, using monthly long-term data (JPL). The methodology in the second line uses the data return maximization method, more suitable for Ka-band links, still using monthly long-term statistics. Finally, the third line introduces the WF approach in the maximization method.

The last column of the table reports the advantage of using WF data: the percentage is the gain (in terms of percentage of received frames) between the WF-based approach and the

TABLE III
SEMI-EMPIRICAL SCENARIO: YEARLY RX 0044V WITH STATISTICAL AND MAXIMIZATION TECHNIQUE FOR PASS AND SUBPASS ANALYSIS TYPE TECHNIQUE

Technique	Database, timescale, analysis type	Yearly rx DV (%)[a]	Yearly mean (%) losses
Statistical (CD=90%)	JPL *Monthly*: pass	ref	0.82
	RMOP *Daily*: pass	102.1	0.61
	JPL *Monthly*: s-pass	118.8	0.91
	RMOP *Daily*: s-pass	123.3	0.71
Maximization (F_{LXth}=5%)	JPL *Monthly*: pass	98.8	0.89
	RMOP *Daily*: pass	106.9	0.69
	JPL *Monthly*: s-pass	103.9	0.73
	RMOP *Daily*: s-pass	124.9	0.76
Benchmark	*Actual time-series*: fully adaptive	208.7	0%

[a] Received data volume: percentage wrt reference case (ref).
Results with JPL monthly and RMOP daily data are compared. Benchmark case is also shown.

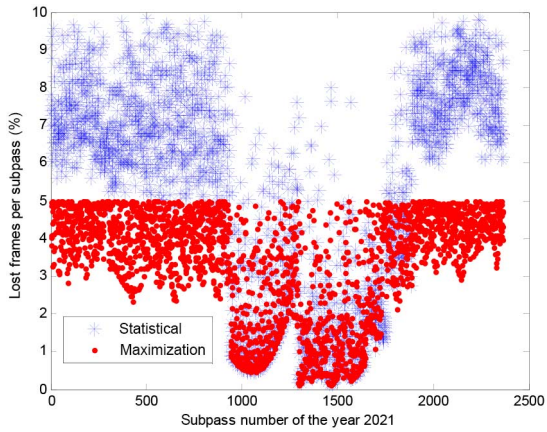

Fig. 11. Expected losses per subpass with statistical and maximization technique (using JPL monthly statistics): statistical technique does not guarantee losses <5%. A saturation effect is evident in subpasses 900–1600.

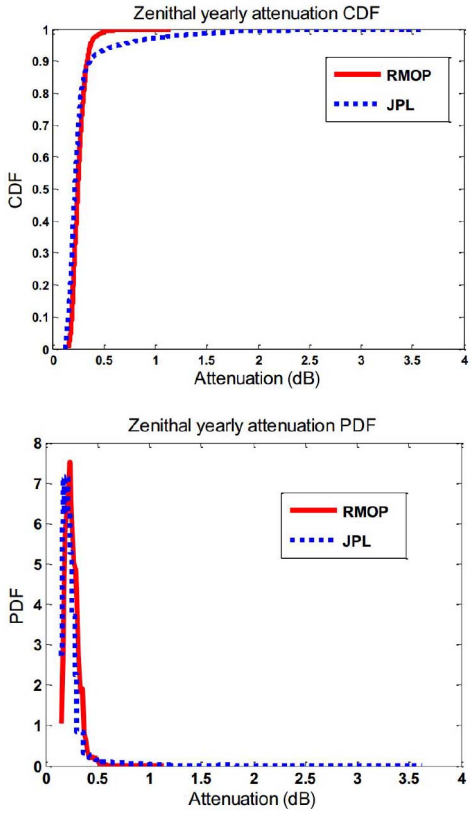

Fig. 12. CDF (top panel) and PDF (bottom panel) of yearly zenithal attenuation from RMOP and JPL data: JPL curves have a larger dynamic. Note that for clarity we reported the yearly statistics but also the monthly ones have a similar trend.

TABLE IV
SEMI-EMPIRICAL SCENARIO: COMPARISON BETWEEN HIGHLIGHTED CASES IN TABLE II METHODOLOGY

Methodology	Technique and Analysis type	Statistical data	WF gain
Standard	Statistical, pass	Monthly–JPL	25%
Advanced	Maximization, s-pass	Monthly–JPL	20%
Potential (WF)	Maximization, s-pass	Daily–RMOP	Reference

In the last column, WF gain in terms of percentage of received data volume (in Table III), with respect to the considered case, is reported.

considered technique. The daily-PDF WF technique can give a gain of about 20%–25% with respect to the reference.

Within the limitation mentioned above due to a single-year WF simulations and the use of SRM as a verification data set, the potential of 20% increase of received data using WF to size the downlink is an appealing result in DS missions.

To conclude, the main considerations linked to the RMOP chain exploitation tend to confirm those derived from the full-numerical scenario analysis.

1) Use of daily-PDF statistics, based on WF, seems to be advantageous with respect to monthly-PDF statistics, based on long-term measurements (up to 20% of annual data volume increase).
2) The advantage of WF-based RMOP is larger in rainy months (April and November in Cebreros, for year 2012).
3) Available JPL statistics of path attenuation results into a dispersion larger than RMOP data mainly due to the longer collecting-time of JPL data.

V. CONCLUSION

The exploitation of WF mesoscale models, coupled with radiopropagation microphysical models, has been illustrated in order to evaluate atmospheric effects at Ka-band for DS mission applications. We have considered two data return estimation techniques, the statistical and maximization algorithms, with stochastic channel downlink characterization to tackle the inherent randomness of the atmospheric wave propagation at Ka-band. We have illustrated the numerical results, in terms of received and lost data, for two analysis scenarios: the full-numerical (a sensitivity test) and the semiempirical (a preliminary verification with measured data). We considered the BC mission as baseline test-case.

The conclusion of this work is that an advanced radio-meteorological forecast-based approach, such as the RMOP concept, is promising. The data volume prediction methods can be trained using daily (or even hourly) time scale to generate *ad hoc* PDF of path attenuation and antenna noise temperature. Predictions based on daily WF-PDF can provide an increase of more than 20% of annual data volume with respect to predictions based on long-term monthly-PDF. The benchmark results are a useful upper limit to the capability of Ka-band downlink channel exploitation. The regional and microphysical fine tuning of the initialization parameters of the mesoscale forecast model (WFM) is also important to better reproduce existing statistics (e.g., JPL radiometric data at Robledo).

Future works will be devoted to overcome the major limitations of the current approach: 1) quantify the impact of RMOP spatial-temporal resolution on data volume transfer; 2) extension of the analysis period to at least 5 years in order to consolidate the statistical significance of the RMOP scores, 3) experimental validation data: foreseen microwave radiometric measurements and radiosonde in Cebreros can be exploited to perform an experimental validation and a fine tuning of MM5-RTM.

ACKNOWLEDGMENT

The authors gratefully acknowledge the precious contribution of M. Gregnanin and M. Parisi (Sapienza University of Rome, Italy, and ARPSOFT srl, Italy) for orbital data analysis and data return evaluation as well as the support of E. Montagnon and M. Arza (ESOC-ESA, Germany) for continuous advising. The authors also thank S. Di Fabio and M. Polsoni (CETEMPS, Italy) and L. Bernardini (HIMET srl, Italy) for their help in data processing and numerical mesoscale model set up.

APPENDIX

A. Satellite Pass and Subpass Definition

In this work, we have distinguished two types of visibility periods: satellite passes and subpasses.

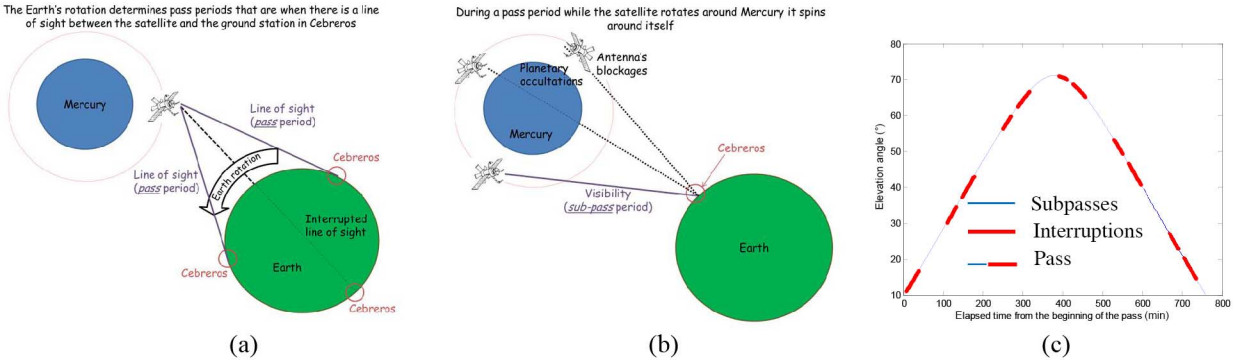

Fig. 13. Passes and subpasses definitions (note that distances and dimensions are not scaled). (a) Passes are determined by Earth rotation that influences the elevation angle under which the ground station in Cebreros points the satellite (determining their line of sight). (b) Subpasses are determined by antenna blockages and planetary occultations that occurs within a pass period. (c) Example of the ground station temporal elevation profile during a pass with relative interruptions and subpasses.

The passes are periods when there is a line-of-sight between the ground station (in Cebreros) and the planet (Mercury), as shown in Fig. 13(a). The subpasses are periods when the ground station is in visibility with the spacecraft that orbits around the planet, as explained in Fig. 13(b). Thus, during a single pass, we have intermittent subpasses caused by the interruption of visibility between the Earth station and the spacecraft. The subpasses can be defined as the set of the periods without interruptions during which data can be effectively received within a given pass. Interruptions can be due to antenna blockages or planetary occultation. The antenna blockages are caused by the satellite motion that, spinning on itself while orbiting around the planet, can block the transmission between the spacecraft antenna and the receiving Earth station [Fig. 13(b)]. The planetary occultation happens when the planet lies in the line of sight between the satellite and the Earth station [Fig. 13(b)].

The satellite passes are determined by the Earth rotation that influences the elevation angle under which the ground station points toward the satellite [determining their line of sight as in Fig. 13(a)]. During a pass period, the elevation angle of the ground station antenna varies (to follow the satellite motion) ranging from a minimum to a maximum value and back from the maximum to the minimum approaching a parabolic shape, as shown in Fig. 13(c). Note that the Earth can occult the transmission when the elevation angle of the Earth station is too close to the horizon; for this reason, for DS spacecraft, each pass can normally be exploited for the data transmission only when the elevation angle is greater than or equal to 10° [Fig. 13(c)].

In Fig. 13(c), an example of the ground station temporal elevation profile during a pass is shown (it goes from minute 0 to minute 759) with relative visibility interruptions and subpasses. Note that the maximum elevation angle in a pass is theoretically 90° (at the zenith) but it depends on the Earth rotation and on the relative position of the Earth with respect to the planet that varies in the different periods of the year. For the BC mission (i.e., for the Cebreros ground station pointing at Mercury), during the year 2021, the maximum elevation angle of satellite passes ranges from values of about 24° to values of about 75°.

The WF approach described in this work can be equally applied to passes or subpasses. The current data transmission strategy for BC avoids the change of data rate during visibility periods which means fixed data rate during a subpass. In this work, the data volume analysis has been performed both at pass and subpass level, in order to assess the benefits of changing the data rate for the different subpasses according to the WF, with respect to a single data rate per pass concept (less operational complexity).

REFERENCES

[1] E. Matricciani, "An optimum design of deep-space downlinks affected by tropospheric attenuation," *Int. J. Satell. Commun. Netw.*, vol. 27, no. 6, pp. 312–329, 2009, doi: 10.1002/sat.942.
[2] F. Davarian, S. Shambayati, and S. Slobin, "Deep space Ka-band link management and mars reconnaissance orbiter: Long term weather statistics versus forecasting," *Proc. IEEE*, vol. 92, no. 12, pp. 312–329, Nov./Dec. 2004.
[3] J. Benkhoff *et al.*, "BepiColombo comprehensive exploration of mercury: Mission overview and science goals," *Planet. Space Sci.*, vol. 58, no. 1–2, pp. 2–20, 2010.
[4] G. Brussaard and P.A. Watson, *Atmospheric Modelling and Millimetre Wave Propagation*. London, U.K.: Chapman & Hall, 1995.
[5] E. Vassallo *et al.*, "The European space agency's deep-space antennas," *Proc. IEEE*, vol. 95, no. 11, pp. 2111–2131, Nov. 2007.
[6] S. Shambayati, "On the benefits of short-term weather forecasting for Ka-band (32 GHz)," in *Proc. IEEE Aerosp. Conf.*, Mar. 2004, pp. 1489–1498.
[7] F. T. Ulaby, R. K. Moore, and A. K. Fung, *Microwave Remote Sensing: Active and Passive*, 1982, vol. I, ch. 5. Reading, MA, USA: Addison-Wesley.
[8] F. S. Marzano, "Modeling antenna noise temperature due to rain clouds at microwave and millimeter-wave frequencies," *IEEE Trans. Antennas Propag.*, vol. 54, no. 4, pp. 1305–1317, Apr. 2006.
[9] F. S. Marzano, "Predicting antenna noise temperature due to rain clouds at microwave and millimeter-wave frequencies," *IEEE Trans. Antennas Propag.*, vol. 55, no. 7, 2022–2031, Jul. 2007.
[10] D. D. Hodges, R. J. Watson, and G. Wyman, "An attenuation time series model for propagation forecasting," *IEEE Trans. Antennas Propag.*, vol. 54, no. 6, pp. 1726–1733, Jun. 2006.
[11] A. Grell, J. Dudhia, and D. R. Stauffer, "A description of fifth-generation Penn State/NCAR mesoscale model (MM5)," National Center for Atmospheric Research, Boulder, CO, US, NCAR Tech. Note NCAR/TN-398+STR, 1994.
[12] K. W. Tao and J. Simpson, "Goddard cumulus ensemble model. Part I: Model description," *Terr. Atmos. Ocean Sci.*, vol. 4, pp. 19–54, 1993.
[13] S. Shambayati, "Ka-band telemetry operations concept: A statistical approach," *Proc. IEEE*, vol. 95, no. 11, pp. 2171–2179, Nov. 2007.
[14] M. Montagna, M. Mercolino, M. Arza, M. Lanucara, E. Montagnon, and E. Vassallo, "Maximization of data return at Ka-band for interplanetary missions," in *Proc. 18th Ka Broadband Commun. Navig. Earth Observ. Conf.*, Sep. 2012, pp. 24–27.

[15] M. Biscarini *et al.*, "Evaluation of deep space Ka-band data transfer using radiometeorological forecast models," in *Proc. Eur. Conf. Antennas Propag. (EuCAP)*, 2014, pp. 499–503.
[16] F. S. Marzano *et al.*, "Investigating Ka-band science data transfer for bepi-Colombo mission by using radiometeorological numerical models," in *Proc. TTC 6th ESA Int. Workshop Track. Telem. Command Syst. Space Appl.*, Sep. 2013, pp. 1–8.
[17] W. Skamarock *et al.*, "A description of the advanced research WRF version 3," National Center for Atmospheric Research, Boulder, CO, USA, NCAR Technical Note NCAR/TN-475+STR, 2008.
[18] The ALADIN Project, "Mesoscale modelling seen as a basic tool for weather forecasting and atmospheric research," *WMO Bull.*, vol. 46, no. 4, pp. 317–324, Oct. 1997.
[19] R. A. Pielke *et al.*, "A comprehensive meteorological modeling system—RAMS," *Meteorol. Atmos. Phys.*, vol. 49, no. 1–4, pp. 69–91, 1992.
[20] C. Gebhardt, S. Theis, P. Krahe, and V. Renner, "Experimental ensemble forecasts of precipitation based on a convection-resolving model," *Atmos. Sci. Lett.*, vol. 9, pp. 67–72, 2008, doi: 10.1002/asl.177.
[21] J. Dudhia, "A nonhydrostatic version for the Penn-State-NCAR mesoscale model: Validation test and simulation of an Atlantic cyclone and cold front," *Mon. Weather Rev.*, vol. 121, pp. 1493–1513, 1993.
[22] J. Reisner, R. J. Rasmussen, and R. T. Bruintjes, "Explicit forecasting of supercooled liquid water in winter storms using the MM5 mesoscale model," *Q. J. R. Meteorol. Soc.*, vol. 124B, pp. 1071–1107, 1998.
[23] S.-Y. Hong and H.-L. Pan, "Nonlocal boundary layer vertical diffusion in a medium-range forecast model," *Mon. Weather Rev.*, vol. 124, pp. 2322–2339, 1996.
[24] I. Troen and L. Mahrt, "A simple model of the atmospheric boundary layer: Sensitivity to surface evaporation," *Bound.-Lay. Meteorol.*, vol. 37, pp. 129–148, 1986.
[25] J. S. Kain and J. M. Fritsch, "Convective parameterization for mesoscale models: The Kain–Fritsch scheme," in *The Representation of Cumulus Convection in Numerical Models, Meteorological Monographs*, Boston, MA, USA: American Meteorological Society, 1993, pp. 165–170.
[26] D. S. Wilks, *Statistical Methods in the Atmospheric Sciences*, 2nd ed. New York, NY, USA: Academic, 2006.
[27] H. Masunaga *et al.*, "Satellite Data Simulator Unit (SDSU): A multi-sensor, multi-spectral satellite simulator package," *Bull. Amer. Meteorol. Soc.*, vol. 91, pp. 1625–1632, 2010.
[28] F. S. Marzano and L. Roberti, "Numerical investigation of intense rainfall effects on coherent and incoherent slant-path propagation at K band and above," *IEEE Trans. Antennas Propag.*, vol. 41, no. 5, pp. 965–977, May 2003.
[29] E. A. Smith *et al.*, "Intercomparison of microwave radiative transfer models for precipitating clouds," *IEEE Trans. Geosci. Remote Sens.*, vol. 40, no. 3, pp. 541–549, Mar. 2002.
[30] F. S. Marzano *et al.*, "Sky-noise temperature modeling and prediction for deep space applications from X band to W band," in *Proc. TTC Conf.*, Sep. 2010, pp. 1–8.
[31] International Telecommunication Union—Radiopropagation (ITU-R), Radio Noise Geneva, Switzerland, ITU-R Rec., pp. 372–377, 2001.
[32] V. Mattioli, F. S. Marzano, N. Pierdicca, C. Capsoni, and A. Martellucci, "Modeling and predicting sky-noise temperature of clear, cloudy, and rainy atmosphere from X- to W-band," *IEEE Trans. Antennas Propag.*, vol. 61, no. 7, pp. 3859–3868, Jul. 2013.
[33] D. Slobin, "DSN telecommunications link design handbook: 105, Rev. D atmospheric and environmental effects," Pasadena, CA, USA: California Inst. Technol., Sep. 2009.
[34] International Telecommunication Union, *Radiopropagation*, ITU-R. Rec., pp. 618–610, 2008.
[35] E. Matricciani, "Rain attenuation predicted with a two-layer rain model," *Eur. Trans. Telecommun.*, vol. 2, no. 6, pp. 715–727, Nov./Dec. 1991 [Online]. Available: http://onlinelibrary.wiley.com/doi/10.1002/ett.4460020615/abstract

Marianna Biscarini (S'15) received the B.Sc. and M.Sc. degrees in electronic engineering from Sapienza University of Rome, Rome, Italy, in 2008 and 2012, respectively.

In 2012, she joined the Department of Information Engineering, Sapienza University of Rome, and the Centre of Excellence CETEMPS, L'Aquila, Italy, to cooperate on radiopropagation, numerical modeling, and microwave radiometry. She is involved with the RadioMetOp project started in 2013.

Frank S. Marzano (F'15) received the Laurea degree (*cum laude*) in electrical engineering and the Ph.D. degree in applied electromagnetics from the University of Rome "La Sapienza," Rome, Italy, in 1988 and 1993, respectively.

In 1992, he was a Visiting Scientist at Florida State University, Tallahassee, FL, USA. During 1993, he collaborated with the Institute of Atmospheric Physics, National Council of Research (CNR), Rome, Italy. In 1997, he joined the Department of Electrical Engineering, University of L'Aquila, L'Aquila, Italy, teaching courses on electromagnetic fields as an Assistant Professor. In 1999, he was at Naval Research Laboratory, Monterey, CA, USA, as a Visiting Scientist. In 2002, he cofounded the Center of Excellence on Remote Sensing and Hydro-Meteorological Modeling (CETEMPS), L'Aquila, Italy. In 2005, he joined the Department of Information Engineering, Electronics, and Telecommunications, Sapienza University of Rome, Rome, Italy, where he currently teaches courses on antennas, propagation, and remote sensing. Since 2007, he has been the Vice-Director of CETEMPS, University of L'Aquila, where he became a Director in 2013. He has authored more than 110 papers on refereed international journals, more than 30 contributions to international book chapters, and more than 230 extended abstract on international and national congress proceedings. He is the Editor of two books. His research interests include passive and active remote sensing of the atmosphere from ground-based, airborne, and space-borne platforms and electromagnetic propagation studies.

Dr. Marzano is a Fellow of the U.K. Royal Meteorological Society and a Member of the MWI-ICI Science Advisory Group of EuMetSat Science Team of NASA. He has been acting as an Associate Editor of the IEEE GEOSCIENCE REMOTE SENSING LETTERS since January 2004 and EGU Atmospheric Measurements Techniques and IEEE-TGRS since 2011.

Mario Montopoli received the Laurea degree in electronic engineering from the University of L'Aquila, L'Aquila, Italy, in 2004, and the Ph.D. degree in radar meteorology within a joint program from the University of Basilicata, Potenza, Italy, and Sapienza University of Rome, Rome, Italy, in 2008.

In 2005, he joined the Center of Excellence (CETEMPS), L'Aquila, Italy as a Research Scientist on ground-based radar meteorology and microwave remote sensing. In 2006, he was a Research Assistant with the Department of Electrical Engineering and Information, University of L'Aquila. From October 2011 to 2013, he was with the Department of Geography, University of Cambridge, Cambridge, U.K., under the Marie Curie FP7 European program. He is currently with the Department of Information Engineering, Sapienza University of Rome and EuMetSat Visiting Scientist at H-SAF facility.

Klaide De Sanctis received the Laurea degree in physics from the University of L'Aquila, L'Aquila, Italy, in 2001, and the Ph.D. degree in atmospheric physics within a joint program from the University of Basilicata, Potenza, Italy, and the University of L'Aquila, in 2008.

In 2002, he joined CETEMPS, University of L'Aquila, as a Research Scientist on extraterrestrial atmospheric dynamics and mesoscale meteorological modeling. Since 2007, he has been with HIMET, L'Aquila, Italy, where he joined the Mesoscale Meteorology Division.

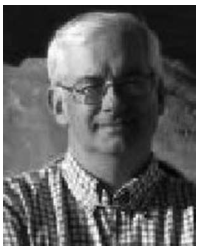

Luciano Iess received the Laurea degree in physics from the University of Pavia, Pavia, Italy, in 1981.

He is currently a Professor of space systems and missions with the Department of Mechanical and Aerospace Engineering (DIMA), University of Rome "La Sapienza", Rome, Italy. He has authored more than 60 papers in peer-review journals and more than 100 papers and abstracts in conference proceedings. His research interests include spacecraft tracking systems, orbit determination, space instrumentation, planetary geodesy, and solar system exploration. He is Principal Investigator of radio science experiments in the ESA missions BepiColombo to Mercury and JUICE to the Galilean moons. He is a team member on NASA's Cassini and Juno missions. He has served for many years in the advisory structure of the European Space Agency and has been Team Leader for the development of the ESA delta-DOR correlator.

Maria Montagna (M'14) received the M.Sc. and the Ph.D. degrees in electronic engineering from the University of Pavia, Pavia, Italy, in 2006 and 2009, respectively.

She joined the Systems and Project Support Section of the European Space Operations Centre (ESOC), European Space Agency (ESA), Darmstadt, Germany, in 2009. Her research interests include ESA concern link budget analyses and optimization of operations concept for TT&C and data volume return, especially for interplanetary missions.

Mattia Mercolino received the M.Sc. degree in aerospace engineering from the University of Rome "La Sapienza," Rome, Italy, in 2002.

From 2002 to 2004, he was with the Aerospace and Astronautic Engineering Department, University of Rome "La Sapienza," where he worked on the radio science experiments onboard Cassini and Smart-1 and on the proposal for the selected more radio science experiment onboard the BepiColombo ESA cornerstone mission to Mercury. In 2004, he joined the European Space Operations Centre (ESOC), European Space Agency (ESA), Darmstadt, Germany, to work on delta-DOR and radio science-related matters.

Marco Lanucara received the Laurea degree in electronic engineering from the University of Rome "La Sapienza," Rome, Italy, in 1994.

In 2000, he joined the Operations Department, European Space Agency (ESA), Darmstadt, Germany, as a Ground Operations Manager, where he has been a System Engineer with the Ground Stations Engineering Division since 2003. His research interests include the analysis and implementation of ESA mission requirements in relation with ground-station development.